International Journal of Science and Research (IJSR)
ISSN (Online): 2319-7064
Index Copernicus Value (2016): 79.57 | Impact Factor (2017): 7.296

Adaptive Fractional-Order Fuzzy Logic Control of Grid-Tied Photovoltaic Inverter

Hamedalneel Babiker Aboh

Indian Institute of Technology Roorkee, Electrical Engineering Department, Roorkee, Uttarakhand 247667, India

Abstract: ***Photovoltaic (PV) energy source has gained more interest in recent decades, due to the environmental concerns and depletion in the conventional energy resources reserve such as fossil fuel. Furthermore, this type of energy source has more advantages such as free of pollution, reliability, availability, no mechanical moving part, little maintenances, has long life time, and quietness. In future more, photovoltaic energy source is anticipated to be interfaced with a grid. Beside the low efficiency of a photovoltaic energy source, a controllability of gird-tied based photovoltaic system its main challenge. As the result, interfacing photovoltaic energy source to grid can derived to grid instability, if the system is not appropriately adjusted. Therefore, the control techniques applied to grid-tied photovoltaic energy source becomes of high interest and always important for the sake of accomplish excellent power quality and highest reliability. Those goals can be accomplished by advanced control methods which includes two stages: The first stage is MPPT controller based on the fractional-order fuzzy logic controller (FOFLC) to accomplish the objective of maximizing the output power of photovoltaic array during regular and irregular atmospheric conditions. A second stage is the control of H-bridge VSI with unipolar sinusoidal pulse width modulation (SPWM) technique. A control technique of the H-bridge VSI consists of two cascaded loops, where an external loop voltage regulator is employed to stabilize voltage of dc link to a required level, this can be achieved by the means of MPPT algorithm, while an internal loop current regulator is employed to maintain the unity power factor operation. It has been found that from many research studies have been done concerning to the grid-tied photovoltaic energy source which mainly focuses on the internal control loop with less attention to external control loop and lacking of stability analysis. This paper presents the complete control techniques of single-phase grid-tied photovoltaic energy source considering the nonlinear dynamic behavior of photovoltaic energy source. For the validation of an effectiveness, efficiency, and validity of the proposed model the simulation results have accomplished through MATLAB/ Simulink simscope power system.***

Keywords: Photovoltaic (PV), grid-tied PV system; FOFLC MPPT, current/voltage controller, phase locked loop (PLL).

1. Introduction

Recently the renewable energy source has gained more interest, due to the environmental concerns and depletion in the conventional energy resources reserve such as fossil fuel [1], [2]. Among all renewable energy source photovoltage energy is preferred. This type of energy source has more advantages such as free of pollution, reliability, availability, no mechanical moving part, little maintenances, has long life time, and quietness [3]. The photovoltaic system exhibits nonlinear dynamic characteristics of (voltage, current), and change with atmospheric conditions (irradiance and temperature). Consequently, a MPPT algorithm technique is employed to ensure that the photovoltaic array is operating at MPP to match the current atmospheric variations [4]. MPPT technique is a real-time control algorithm, which applied to energy converter placed between photovoltaic module and photovoltaic inverter to amplify the photovoltaic module output power. Numerous MPPTs algorithm techniques have studied and industrialized in recent decades to increase the efficiency operation of the photovoltaic module during varying atmospheric conditions [4], [5]. In this study fractional order fuzzy logic controller based MPPT techniques is integrated to the system to maintain the photovoltaic array operation at MPP regardless of the atmospheric conditions. The advantages of this technique are: fast dynamic response; control imprecise system; robustness; needless of exact mathematical expression [6]. Moreover, this technique has ability to precisely track the MPP with minimum oscillation under rapidly atmospheric conditions compare to the classical MPPT algorithms such incremental conductance (INC), and perturbation and observation (P&O) [7]. Due to the advanced improvement in the power electronics devices, a market of the PV system interfaced to the utility grid is steadily increasing. Nevertheless, the PV system suffers from low efficiency, as result interfacing of photovoltaic energy source to a utility grid can derive instability problem, if the system is not appropriately designed [8], [9]. Therefore, the control scheme applied to grid-tied PV energy generation system becomes of high interest. Usually VSI with unipolar SPWM is most widely used in the grid-tied PV system because of its simplicity, fast-dynamic response, and high-power factor. The control scheme of a H-bridge voltage source photovoltaic inverter with unipolar SPWM, which consists of two cascade control loops: an external loop voltage regulator is responsible for the stability of voltage at dc link, and an internal loop current controller is employed to produce the duty cycle of a VSI to generate sinusoidal current and voltage as well as to maintain the system unity power factor operation. To reduce the switching frequency ripples injected into grid associated with output current of PV inverter, LCL-filter is used [10]. The aforementioned control scheme should be designed at highest possible reliability to meet the utility grid requirements and regulations that recommended by IEEE-519 and IEC-61727 standards. The IEEE-519 standards stated that the permissible THD in PV inverter output current must be lower than 5%, with individual limit of 4% for every odd harmonic from 3rd to 9th and 2% from 11th to 17^{th} [11], [12]. Those issues are the main part of this study. The IEEE-519

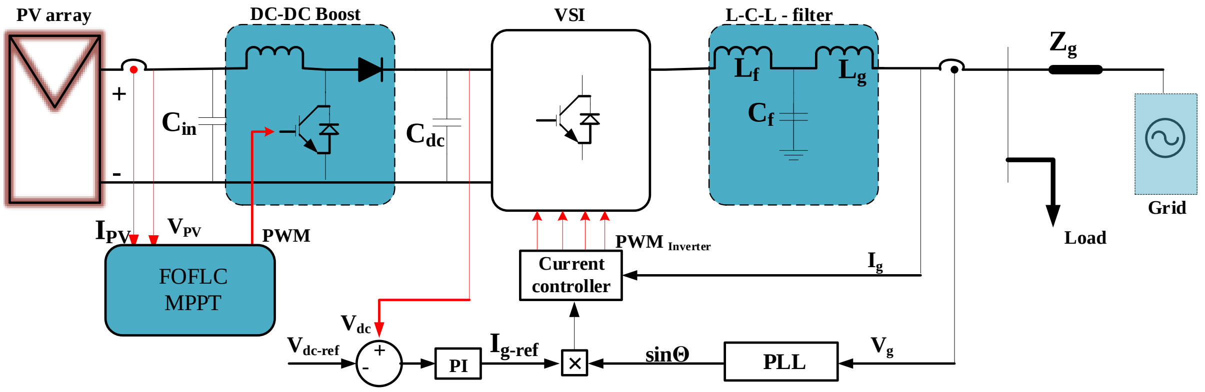

Figure 1: Schematic representation of dual-stage single-phase grid-tied photovoltaic system.

2. System Configuration

A Schematic representation of the proposed dual-stage grid-tied single-phase PV system is illustrated in Fig. 1, which consists of PV array, the dc-dc boost converter, the MPPT based on Fractional order fuzzy logic controller, H-bridge unipolar SPWM VSI inverter, single-phase LCL filter, and grid synchronization algorithm based on the phase locked loop (PLL).

3. FOFLC Based on MPPT

The main goal of a FOFLC based on MPPT technique in a PV energy source is to regulate constantly operation of PV module at MPP irrespective of the variations of the atmospheric conditions [9]. The FOFLC-based MPPT offers adaptive variations of the duty ratio based on the position of the operating point regrading to maximum power point Hence, this can decrease the steady-state oscillation and power functionating problems under quick variations in atmospheric conditions. Nevertheless, although the excellent performance of FLC technique in tracking an MPP, but also it has some limitations such as fixed on fuzzy field [13], deep experience of the system operation, and requires large memory size with high-speed microcontroller ability with large memory size. Fractional order-FLC (FOFLC) is proposed to enhance the tracking in case of the varying atmospheric conditions, by comprehend the precision of a FLC with robustness the of an FO. As the result the FOFLC fast-tracks the MPP and prevents deviating from the MPP.
A FLC has two input variables error E(j) and change in error ΔE(j) described as in (1) and one output is change in the duty ratio ΔD(j) of power converter (boost converter).

$$E(j)=\frac{P(j)-P(j-1)}{V(j)-V(j-1)} \qquad (1)$$

$$\Delta E(j)=E(j)-E(j-1)$$

The fraction derivatives of the Gr¨unwald–Letnikov (GL) and Riemann–Lioville definition are commonly used in an FO system. Based on the GL equation which is documented in [14].

$$\frac{d^{\alpha}P(V)}{dV^{\alpha}}=\lim_{\Delta V\to 0}\frac{1}{\Delta V^{\alpha}}\times\sum_{k=0}^{\infty}\frac{(-1)^{k}\Gamma(\alpha+1)}{\Gamma(j+1)\Gamma(\alpha-j+1)}P(V-j\Delta V) \quad (2)$$

Where P(j) indicates as the PV array output power at sample time (j), and V(j) indicates as an output voltage PV array when α > 0. (2) can be modified as in (3) by take into account the only first two terms.

$$\frac{d^{\alpha}P(V)}{dV^{\alpha}}\approx\lim_{\Delta V\to 0}\frac{P(V)-\alpha P(V-\Delta V)}{\Delta V^{\alpha}} \qquad (3)$$

Variations of a voltage and power describe the fair calculation in fractional order calculus. The power (P) and the voltage (V) are at current step. The FO incremental variations of a P and a V are approximated as dαP ≈ P-αP0 and dVα ≈ ΔVα= V-αV0 respectively. Therefore, the (1) can be written as in (4).

$$E(j)=\frac{P(j)-P(j-1)}{V(j)-V(j-1)}=\frac{P-\alpha P_0}{(V-V_0)^{\alpha}} \qquad (4)$$

$$\Delta E(j)=E(j)-E(j-1)$$

Here 0 < α ≤ 1, Once α = 1, represents a FLC. Once 0 < α < 1, signifies a FOFLC [15]. Fig 2 illustrate the geometric estimation of ΔV to the αth derivative, the vertical-axis presents the output power while a horizontal-axis indicates as an output voltage, the third line is α. The fractional order variation of the output power equal to P(V)−αP(V−ΔV). A fractional order variation of an output voltage equal to (αth) differentiate of (ΔV).

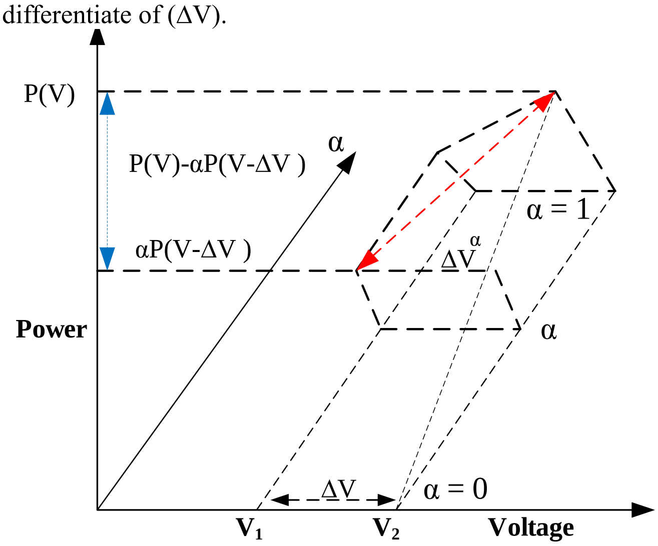

Figure 2: Geometric interpretation of FO differentiation.

Generally, FLC contains of four stages: 1) fuzzification; 2) rule base; 3) inference mechanism; and 4) defuzzification.
In a fuzzification stage the numerical inputs used to describe the control rules are transformed into linguistic variables. A membership functions of the linguistic variables are appointed with five fuzzy subsets as illustrated in Fig 3.

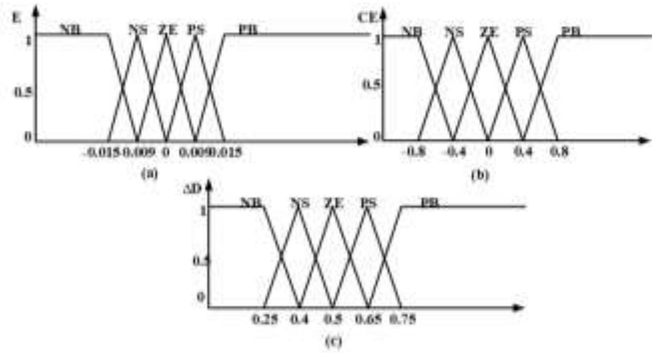

Figure 3: Membership function of (a) E(j), (b) CE(j), (c)and ΔD(j).

By using these membership functions and division of fuzzy subsets, handling efforts to obtain the output control can be diminished drastically, though the steady state oscillation is kept small. Once an input values of FLC E(j) and CE(j) are transformed to the linguistic variables, fuzzy logic output ΔD (j) can be look up in rule base table. The rule base is framed by using fuzzy inference system (FIS) as given in TABLE 1.

TABLE 1: Control rules table of the FOFLC.

E \ CE	NB	NS	ZE	PS	PB
NB	ZE	ZE	PS	NS	NS
NS	ZE	ZE	ZE	NS	NB
ZE	PB	PS	ZE	NS	NB
PS	PB	PS	ZE	ZE	ZE
PB	PB	PS	NS	ZE	ZE

The design strategies of FOFLC are explained as following. First, for an error E(j) and change in error ΔE(j), and an output duty ratio ΔD(j) are depend on the dc-dc converter in addition to on the information of experts. As an example, if the E(j) is the positive big (PB) and CE(j) is negative big (NB) then the ΔD (j) is positive big (PB), this means "if the operating point is distance from the MPP increment the duty cycle largely". Defuzzification is last stage of FLC which the linguistic variables are transformed to numerical variables. Secondary, the center of gravity scheme (COG) is applied to transform fuzzy subsets membership (variation in the duty cycle) to the actual numbers.

$$\Delta D = \frac{\sum_{i}^{N} \mu(D_i) D_i}{\sum_{i}^{N} \mu(D_i)} \tag{5}$$

The output of FOFLC offers an analog signal that is control through PWM which gives ΔD to step up power converter

4. An external Voltage Regulator

The main goal of an external regulator is to adjust the voltage of dc link to a desired level. Generally, dc-link voltage with voltage ripple of 1-5% of the dc-link rated voltage is allowed. Fig 4 illustrates a block diagram of an external loop voltage regulator.

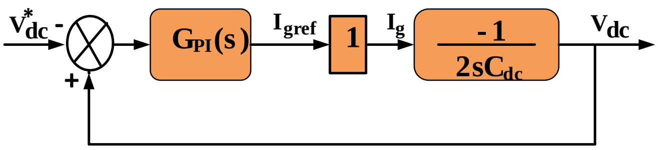

Figure 4: An external voltage regulator block diagram.

Here the reference dc-link voltage compares to actual value of dc-link voltage, and their difference (error) is passed through PI controller to minimize the steady state oscillation [16]. The PI controller for an external loop voltage regulator is expressed by

$$G_{PI}(s) = K_P + \frac{K_i}{s} \tag{6}$$

Where K_P indicates as proportional gain; K_i indicates as integral gain of PI controller. The PI controller for external loop is properly designed for a low crossover frequency (5-20Hz) using Ziglar-Nicholes technique with (K_P *=0.01*, K_i *=0.5*) in order to attenuate the value of (100Hz) that is fedback from dc link. The mathematical expression between the mean voltage of dc-link and the differences in the fundamental grid current magnitude can be determined by means of peak power balance concepts, by neglecting the losses of the converter. The mathematical derivation of the plant transfer function is documented in [17] and repeated here for the purpose of the completeness.

$$G_{Plant}(s) = \frac{V_{dc}(s)}{I_g(s)} = -\frac{1}{2sC_{dc}} \tag{7}$$

5. An internal Current Regulator

Typically, the current regulator is applied to achieve high power quality, stability, which are very significant matters for responding with the standards. Usually, the dynamic response of an internal current regulator is faster than the dynamic response of an external voltage regulator. The proportional plus resonant controller (PR) and PI controller with feedforward grid voltage are commonly used in an inner loop current regulator for photovoltaic inverters. However, the PR controller has superiority over PI controller when adjusting the sinusoidal signals. The former controller has ability to remove phase angle steady-state oscillation with needless the voltage feedforward, as well it has capability of disturbance rejection [18], [19]. Due to the harmonic rejection capability and fast dynamic response of PR controller is considered in this study. Fig 5 represents a block illustration of non-ideal PR controller and its transfer function is given in (8).

$$G_{PR}(s) = K_P + \frac{2K_{ri}\omega_c s}{s^2 + 2\omega_c s + \omega_o^2} \tag{8}$$

Where the K_P indicates as proportional, and K_{ri} indicates as resonant gain of PR controller, is ω_c frequency, and is grid frequency.

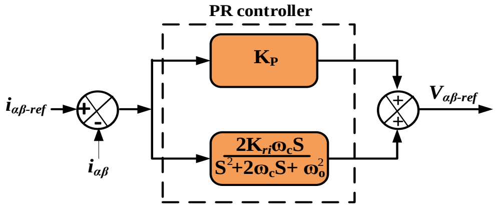

Figure 5: Non-ideal PR controller block diagram.

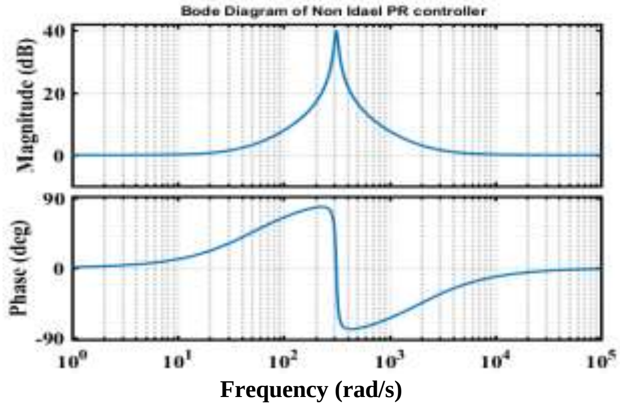

Figure 6: Non-ideal PR controller bode plot.

Fig 4.10 illustrates non-ideal PR controller bode plot (K_p = 1, K_{ri} = 100, ω_c = 10 rad/sec, and ω_0 = 314 rad/sec) with 40 dB finite gain which is highly acceptable for removing the voltage error tracking.

6. Single-Phase Grid Synchronize algorithm

Grid synchronization algorithm presents an essential role in the control of a grid-tied photovoltaic system inverters. Moreover, the parameters of utility grid voltage e.g. (frequency, phase, and amplitude) can be calculated to observer the differences of grid voltage. Various number of the synchronization algorithms such as (park transformation, transport delay T/4, inverse park transformation, and Hilbert Transformation) have been studied and developed in literature [20], [21], [22]. Nevertheless, all these PLL techniques have some drawbacks (i.e. nonlinearity, frequency dependency, complexity) as specified in the [21]. Therefore, in this study PLL technique e based on second order generalized integrator (SOGI) for OSG is used as a substitutional solution to mitigate the abovementioned disadvantages of a conventional PLL techniques. Fig 7 shows a schematic representation of the PLL based on a SOGI-OSG. The SOGI transfer functions are given by

$$G_{SOGI}(S) = \frac{\omega s}{s^2 + \omega^2} \quad (9)$$

$$G_d(S) = \frac{V_g'(s)}{V_g(s)} = \frac{k\omega s}{s^2 + k\omega s + \omega^2} \quad (10)$$

$$G_q(S) = \frac{qV_g'(s)}{V_g(s)} = \frac{k\omega s}{s^2 + k\omega s + \omega^2} \quad (11)$$

Form (9-11) it is clear that the bandwidth of SOGI is the closed loop gain (K) function, and it does not depend on center frequency ω, which makes this technique appropriate for variable frequency operations. In this study the value of K was set equal to 0.7

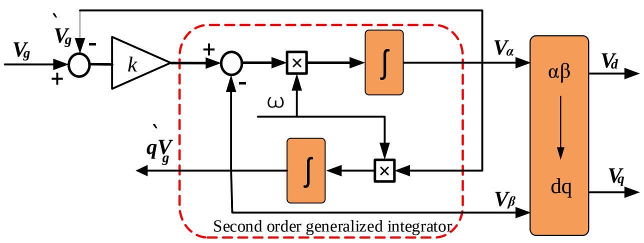

Figure 7: Schematic representation of PLL based on SOGI-OSG.

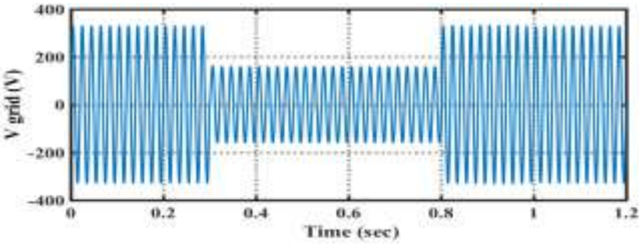

(a)

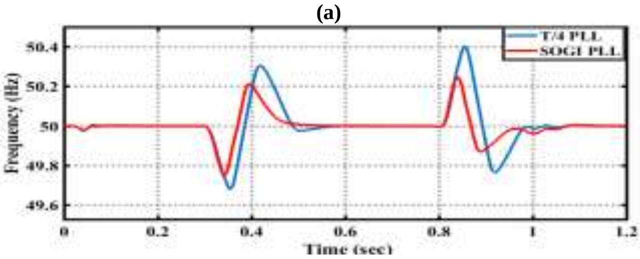

(b)

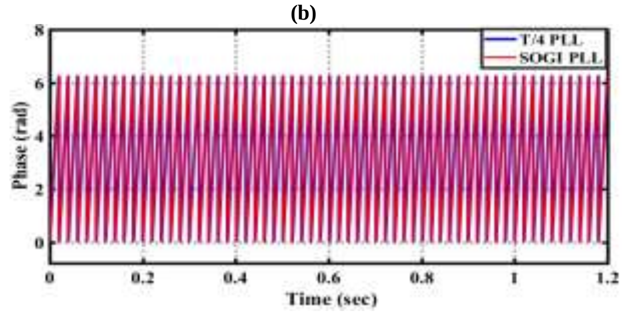

(c)

Figure 8: Comparison of SOGI-OSG based PLL and T/4 transport delay-PLL (a) grid voltage (V) (b) grid frequency (c) Phase of the grid voltage.

In order to make comparison over the overmentioned PLL algorithms the simulation results have done by the means of MATLAB/simulink in case of grid-fault in order to find out the greatest appropriate algorithm for synchronization of grid-interfaced photovoltaic energy source. The results given in Fig 4.18 When the grid is subjected to the fault (voltage sag 0.5 pu). It is clear that from Fig 8 (b) the transport delay (T/4) synchronization algorithm technique is not good when grid is exposed to the frequency differences but this technique can follow when the amplitude changes quickly. Therefore SOGI-OSG tracks an input signals with high efficiency compared to transport delay (T/4) based PLL once utility grid subjected to frequency variations. From the above discussion it is confirmed that the SOGI-OSG gives significantly better results as compared with transport delay (T/4) based PLL.

7. Single-Phase LCL Filter

Generally, the LCL filter is interfaced at the PV inverter output to mitigate the switching harmonics injected into the utility grid [23], [24]. An equivalent electrical circuit configuration of the single-phase LCL filter is illustrated in Fig. 9, which consist of L_f is the inductor of the inverter side L_g is the inductor of the grid side, and C_f is filter capacitor. By considering the inverter as harmonics generator and grid as short circuit the current harmonics attenuation can be calculated. The design procedures of LCL filter values use a line frequency, inverter power rating, and switching frequency as inputs parameters [24]. The LCL values are stated as percentage of the base values.

an LCL-filter transfer function includes damping resistance is given by

$$G_{LCL}(s) = \frac{1}{(L_f L_g C_f)s^3 + C_f (L_f + L_g) R_f s^2 + (L_f + L_g)s} \quad (12)$$

The base capacitor and base impedance can be calculated as in (13)

$$Z_b = V_r^2 / P_r, \; C_b = 1 / \omega_g \times Z_b \quad (13)$$

Where V_r is rated voltage (RMS), P_r is rated power (W), and ω_g is grid frequency. Since the unipolar SPWM is used; hence the inverter side ind-uctor is given by

$$L_c = \frac{V_{dc}}{8 \times \Delta i_{fc\,max} \times f_s} \quad (14)$$

Where f_s is switching frequency , Δi_{fc} is cuurnt ripple. The desierd ripple current is given by

$$\Delta i_{lf\,max} = ripples\% \times \frac{P_r \sqrt{2}}{V_r} \quad (15)$$

The filter capacitor can be calculated as given in (19)

$$C_f = x.C_b \quad (16)$$

Where x represents the percentage of the reactive power required by C_f (in this paper x is taken 5%).
The grid side inductor can be calculated using resonant frequency ($\omega_r = 2\pi f_r$) .

$$\frac{f_s}{2} > f_r > \frac{f_s}{4} \quad (17)$$

$$L_{fg} = \frac{L_{fc}}{\left(\omega_r^2 \times L_{fc} \times C_f\right) - 1} \quad (18)$$

An LCL filter design procedures mentioned above has been applied to system with rated power P_r = 2.7Kw, switching frequency f_s = 10 KHz, rated voltage V_r = 230V (RMS), and dc-link voltage V_{dc} = 400V gives the LCL filter values as given in TABLE 2.

8. Simulation Results and Discussion

For the validation of reliability, accuracy, adequacy, and the efficiency of a proposed system, simulations outcomes are obtained. Moreover, to verify an efficiency and reliability of a proposed MPPT algorithm based FOFLC technique and control techniques of a single-phase grid-interface VSI, have carried out by means of MATLAB/Simulink Simscape power system under three different atmospheric conditions.

8.1 Case one: at standard test condition (STC) 1000 W/m^2 and 25^{0}C.

Fig 8 illustrates the simulation results of the dual-stage system at STC (1000W/m2, 250C). The dc-link voltage regulator adjusts the voltage of a dc link in a short period (t = 0.09 sec) with minimum steady state oscillation as given in Fig 8 (a). It can be noticed that as its given in Fig 8 (b) and (c) an output sinusoidal waveforms of output voltage and current, where both are in-phase. The average active and reactive powers generated by PV system at STC (1000W/m^2, 25^{0}C) are about 2.7 kW and 0 Var as shown in Fig 8 (d). In this situation the inverter is injecting an active power into grid by controlling the d-axis current, and the current of the q-axis is made to be zero at similar time to maintain the reactive power at zero value.

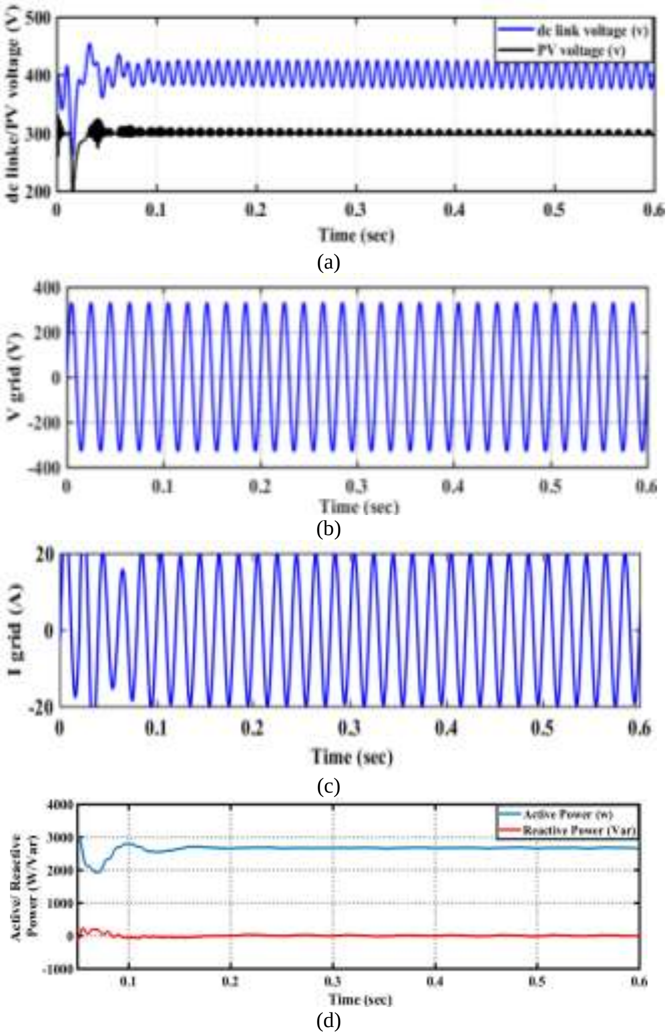

Figure 9: (a) dc link voltage (b) grid voltage (c) grid current (d) Active/ Reactive power.

Fig 10 illustrates an LCL-filter impacts on of a PV inverter output current and output voltage. The FFT plot of a harmonic spectrum and grid current THD is illustrated in Fig 11. Its shows lower harmonic content for inverter output current which is satisfy the IEEE standards. Therefore, the proposed system successfully injected the maximum power into utility grid with nearly unity power factor and high efficiency.

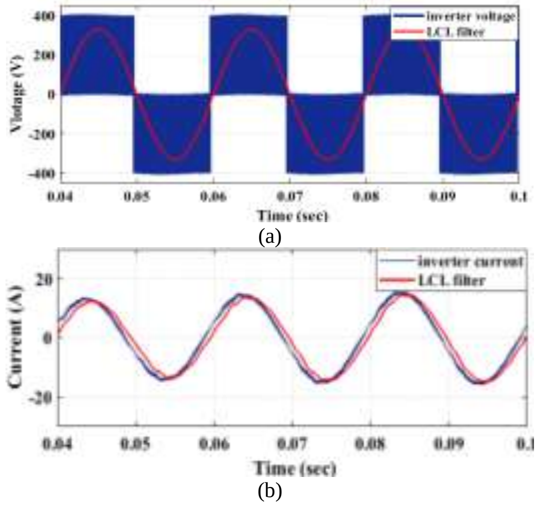

Figure 10: Inverter output (a) voltage (b) current before and after LCL filter.

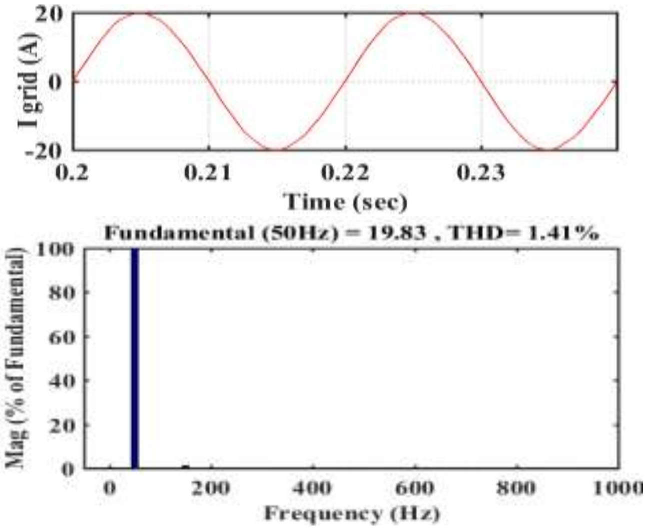

Figure 11: Harmonic spectrum and THD of grid current.

8.2 Case two: at irregular solar irradiance and constant temperature 25^{0}C.

In this situation the simulation results have carried out under irregular solar irradiance and constant temperature. At the beginning the surface temperature was kept constant at 25^{0}C and the initial solar irradiance is considered as 1000W/m^2 the corresponding active and reactive power is 2.7 kW and 0 Var respectively. At t = 0.4 sec, solar irradiance is ramped down from 1000W/m^2 to 500W/m^2 the corresponding decrease in output current and active power equal 1.3 kW but reactive power is kept equal zero as shown in Fig 12 (a), (g). Regardless of change in the solar irradiance the dc link voltage is rapidly stabilized at its desired level of 400 V, which confirms the efficiency and reliability of an external voltage regulator and MPPT algorithm as depicted in Fig 12 (b). At t = 0.8 sec the solar irradiance starts increasing from 500W/m2 to 1000W/m2 corresponding increase in the output current, voltage, and active power (2.7 kw), but the reactive power is remaining constant zero. An external voltage regulator is appropriately track the d-q axis references current as given in Fig 12 (h). An inverter output voltage and current waveforms that injected into utility grid are given in Fig 12 (c), (d), (e). the injected voltage into grid was pure sinusoidal with frequency of 50 Hz and amplitude of 330 V as depicted in Fig 12 (f).

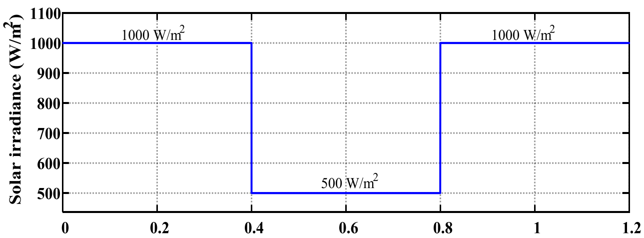

(a)

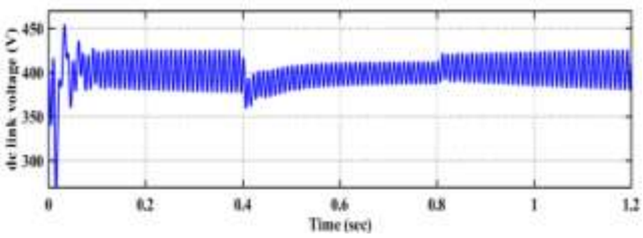

(b)

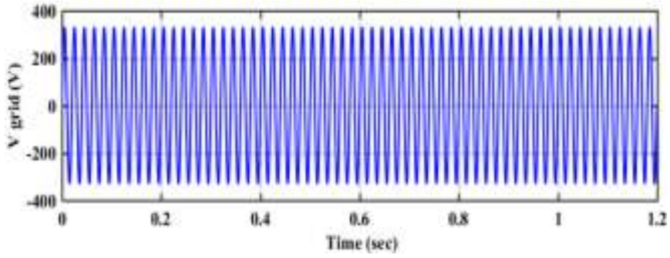

(c)

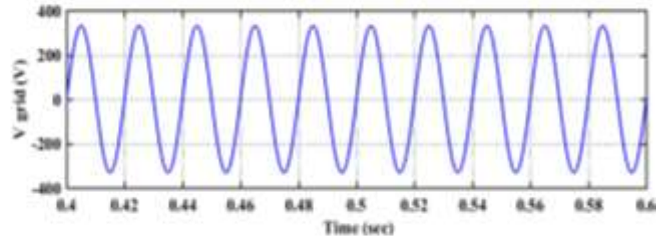

(d)

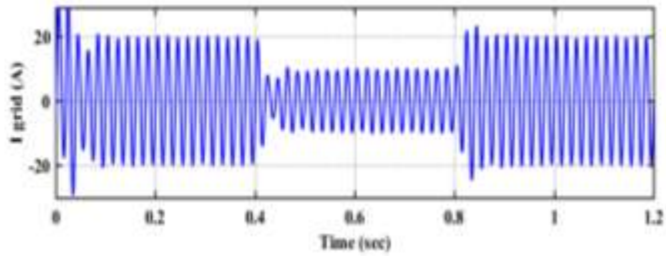

(e)

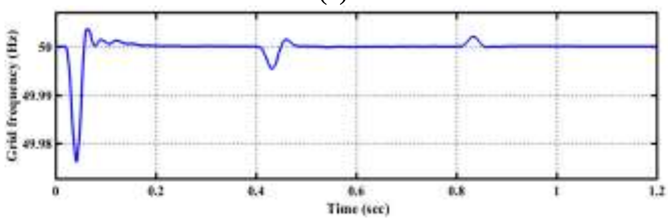

(f)

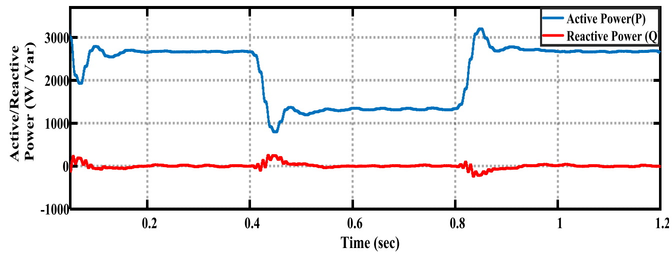

(g)

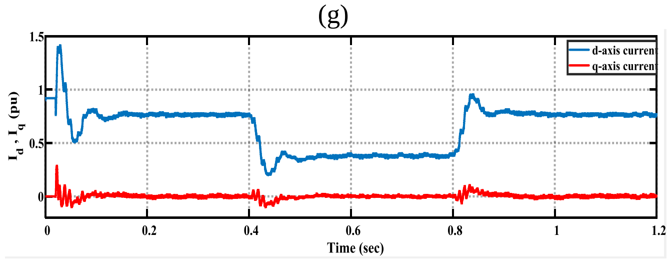

(h)

Figure 12: System responses for the variations of solar irradiance (a) solar irradiance change level (W/m2), (b) dc link voltage (V), (c) grid voltage (v), (d) grid voltage at t = (0.4 sec-0.6 sec), and (e) grid current (A) (f) grid frequency (g) active/reactive power (w/var) (h) d-q axis current (pu).

The grid current and voltage both are in-phase. Therefore, the THD of an inverter output current is less than 5%, which is satisfy the IEEE- 519 standards as shown in Fig 13.

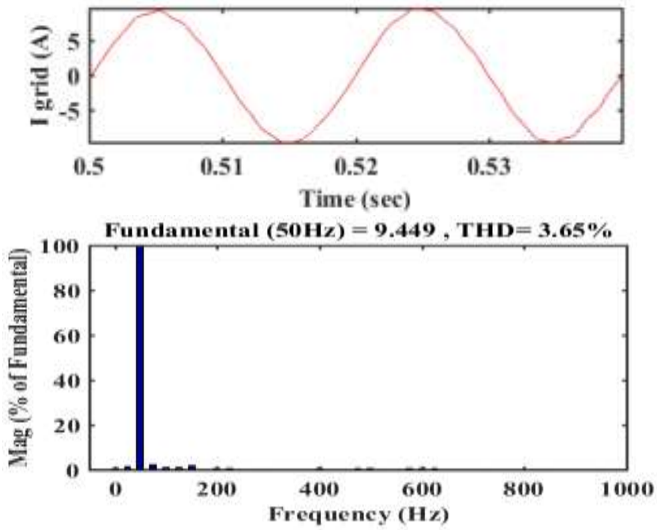

Figure 13: Harmonic spectrum and THD of grid current.

8.3 Case three: at irregular solar irradiance and surface temperature variations

In this case the simulation results have carried out under solar irradiance level variations and surface temperature variations of the PV array. Initially the solar irradiance is set to 1000 W/m^2 and surface temperature is considered as 25^{0}C as represented in Fig 14 (a), (b) it easily to be observed that, the voltage at dc link stabilized at desired level 400 V as shown in Fig 14 (c). At the t = 0.4 sec the PV array is subjected to the lower temperature (25^{0}C) and lower solar irradiance (500 W/m^2), it can be noticed from Fig 14 (c) an external voltage regulator adjusts the voltage at desired level with the help of the FOFLC MPPT algorithm. PV array surface temperatures increase linearly from 25^{0}C to 35^{0}C during the period of 0.7 to 0.8 sec as in Fig 14 (a), (b), also it is easy to notice that the voltage of dc link is still stable as given in Fig 4.28 (c) which demonstrate which confirms the effectiveness and accuracy of proposed MPPT controller and an external dc link voltage regu-lator. An inverter output current and voltage injected into grid is illustrated in Fig 14 (d), (e).

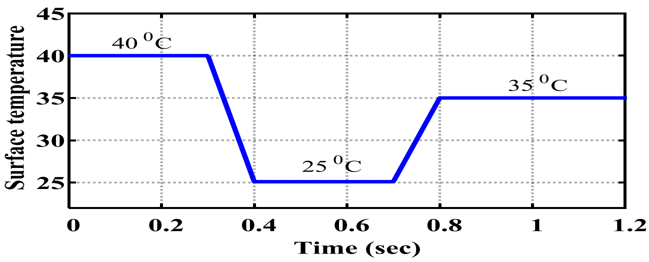

(a)

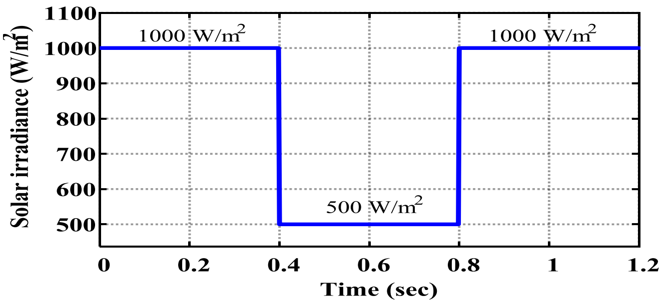

(b)

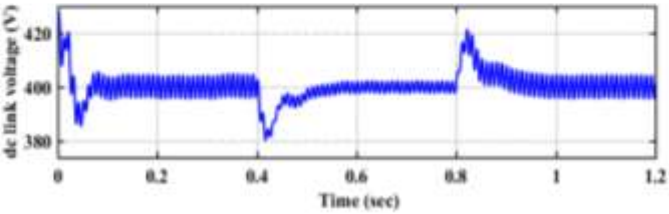

(c)

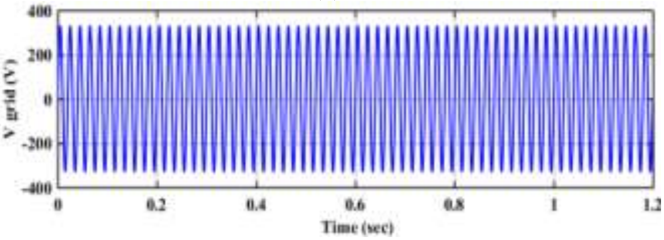

(d)

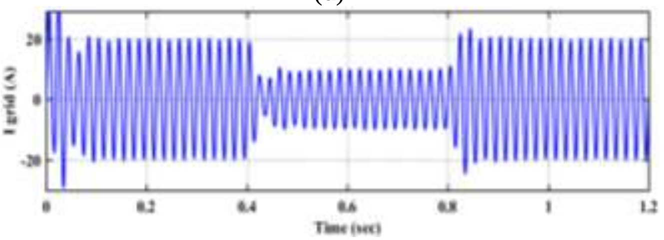

(e)

Figure 14: System responses for the variations of (a) surface temperature variation (b) and solar irradiance variation level (W/m2), (c) dc-Link voltage (V), (d) grid voltage (v), (e) grid current (A).

9. Conclusion

In this paper a dual-stage grid-tied PV system generation and its control schemes have been proposed. The control schemes of the proposed system involve of MPPT algorithm, dc link voltage controller, and current controller. The MPPT technique based on the FOFLC is applied to the PV array for extraction the maximum power, while an external voltage controller is used to adjust the dc link voltage at a desired value. Evaluation of MPPT based FOFLC, voltage and current controller, and grid-side filter for different operation modes have been discussed. From above discussion and simulation results of a proposed system, it has been demonstrated that the control techniques offer better performance with nearly unity power factor under standard test condition (1000W/m^2, 25^{0}C) and changing atmospheric conditions.

References

[1] E. Romero-Cadaval, G. Spagnuolo, L. G. Franquelo, C. A. Ramos-Paja, T. Suntio, and W. M. Xiao, “Grid-connected photovoltaic generation plants: Components and operation,” IEEE Industrial Electron Magazine, vol. 7, no. 3, pp. 6–20, 2013.

[2] J. Guerrero, F. Blaabjerg, T. Zhelev, K. Hemmes, E. Monmasson, S. Jeme??, M. P. Comech, R. Granadino, and J. I. Frau, “Distributed generation: Toward a new energy paradigm,” IEEE Industrial Electronics Magazine., vol. 4, no. 1, pp. 52–64, 2010.

[3] M. Liserre, T. Sauter, and J. Y. Hung, “Future energy systems: Inegrating renewable energy into the smart power grid through industrial electronics,” IEEE

Industrial Electron Magazine., vol. 4, no. March, pp. 18–37, 2010.

[4] B. Subudhi and R. Pradhan, “A comparative study on maximum power point tracking techniques for photovoltaic power systems,” IEEE Transactions. Sustain. Energy, vol. 4, no. 1, pp. 89–98, Jan. 2013.

[5] N. E. Zakzouk, Ahmed K. Abdelsalam, Ahmed A. Helal, and Barry W. Williams, “PV Single-Phase Grid-Connected Converter DC-Link Voltage Sensorless Prospectivo,” IEEE Transactions. Power Electronics., vol. 5, no. 1, pp. 526-546, Mar 2017.

[6] P. L. C. et al. T. Esram, “Comparison of photovoltaic array maximum power point tracking techniques,”,” IEEE transactions energy conversion, vol. 22, no. 2, pp. 439–449, 2007.

[7] R. R. Jha and S. C. Srivastava, “Fuzzy Logic and ANFIS controller for grid integration of Solar PhotoVoltaic,” 2016 IEEE 6th intertional conference on power system. ICPS 2016, 2016.

[8] R. Peña-Alzola, M. Liserre, F. Blaabjerg, M. Ordonez, and Y. Yang, “LCL-filter design for robust active damping in grid-connected converters,” IEEE transactions industrial informatics, vol. 10, no. 4, pp. 2192–2203, 2014.

[9] F. Blaabjerg, R. Teodorescu, M. Liserre, and A. V. Timbus, “Overview of Control and Grid Synchronization for Distributed Power Generation Systems,” IEEE Transactions industrial Electronics., vol. 53, no. 5, pp. 1398–1409, 2006.

[10] International Electrotechnical Commission, “Characteristics of the utility interface for photovoltaic (PV) systems,” IEC 61727, 2004.

[11] N. Vazquez, J. Vazquez, J. Vaquero, C. Hernandez, E. Vazquez, and R. Osorio, “Integrating Two Stages as a Common-Mode Transformerless Photovoltaic Converter,” IEEE Trans. Ind. Electron., vol. 64, no. 9, pp. 7498–7507, 2017.

[12] C. K. Duffey and R. P. Stratford, “Update of Harmonic Standard Ieee-519: Ieee Recommended Practices and Requirements for Harmonic Control in Electric Power Systems,” IEEE Transaactions industrial application., vol. 25, no. 6, pp. 1025–1034, 1989.

[13] N. Zhang, H. Tang, and C. Yao, “A systematic method for designing a PR controller and active damping of the LCL filter for single-phase grid-connected PV inverters,” Energies, vol. 7, no. 6, pp. 3934–3954, 2014.

[14] M. Chengbin and H. Yoichi, “Fractional-order control: theory and applicationsin motion control,” IEEE industrial electronics. Magazine., vol. 1, no. 4, pp. 6–16, Winter 2007.

[15] S. Tang, Y. Sun, Y. Chen, Y. Zhao, Y. Yang, and W. Szeto, “An Enhanced MPPT Method Combining Fractional-Order and Fuzzy Logic Control,” IEEE jornal photovoltaics, vol. 7, no. 2, pp. 640–650, 2017.

[16] N. E. Zakzouk, Ahmed K. Abdelsalam, Ahmed A. Helal, and Barry W. Williams, “PV Single-Phase Grid-Connected Converter DC-Link Voltage Sensorless Prospective,” IEEE Transactions power electronics., vol. 5, no. 1, pp. 526-546, Mar 2017.

[17] Y. Yang, F. Blaabjerg, and Z. Zou, “Benchmarking of grid fault modes in single-phase grid-connected photovoltaic systems,” IEEE Transactions industrial applications., vol. 49, no. 5, pp. 2167–2176, 2013.

[18] V. Sharma, R. Kumar, and N. Tripathi, “Current mode Controller Design for Single Phase grid connected Inverter Using Proportional Resonant Control Strategy,” International jornal emerging technology. Eng., vol. 2, no. 8, pp. 125–130, 2015.

[19] D. K. V. Sagiraju, Y. P. Obulesu, and S. B. Choppavarapu, “Dynamic performance improvement of standalone battery integrated PMSG wind energy system using proportional resonant controller,” Engineering. science technology an international jornal., vol. 20, no. 4, pp. 1353–1365, 2017.

[20] Y. Yang, F. Blaabjerg, and Z. Zou, “Benchmarking of grid fault modes in single-phase grid-connected photovoltaic systems,” IEEE transactions industrial application., vol. 49, no. 5, pp. 2167–2176, 2013.

[21] R. Teodorescu, M. Liserre, and P. Rodriguez, Grid Converters for Photovoltaic and Wind Power Systems. Hoboken, NJ, USA: Wiley, 2011.

[22] R. M. Santos Filho, P. F. Seixas, P. C. Cortizo, L. A. B. Torres, and A. F. Souza, “Comparison of three single-phase PLL algorithms for UPS applications,” IEEE transactions industrial electronics., vol. 55, no. 8, pp. 2923–2932, Aug. 2008.

[23] J. Dannehl, C. Wessels, and F. W. Fuch,” Limitations of voltage-oriented PI current control of grid-connected PWM rectifiers with LCL filter,” IEEE transactions industrial electronnics., vol. 56, no. 2, pp. 380-388, Feb 2009.

[24] M. Liserre, F. Blaabjerg, and S. Hansen, “Design and control of an LCL-filter-based three-phase active rectifier,” IEEE transactions industrial application., vol. 41, no. 5, pp. 1281–1291, 2005.

Author Profile

Hamedalneel Babiker received the B.Sc. degree in electrical and electronic enginee-ring (Power system) from university of Nyala, Nyala, Sudan, in 2014, and the M-tech from Indian Institute of Technology Roorkee, Roorkee, UK, India, in 2018. In 2014 he joined the University of Nyala, electrical engineering department, as teaching assistance and then he became a lecturer in 2018. He has authored three technical papers in referred journal and conferences. His research interests include control of grid interfaced photovoltaic (PV) system, power electronics, power quality, control system, FACTS devices, power system protection, and distributed generation.